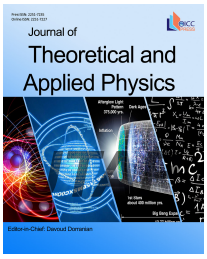

Volume 19, Issue 2, 192523 (1-10)

Journal of Theoretical and Applied Physics (JTAP)

https://doi.org/10.57647/j.jtap.2025.1902.23

Synthesis of formic acid using anodic plasma electrolysis

Triana Devi Sijabat[1], Nelson Saksono[1,*], Bening Farawan[2]

[1]*Department of Chemical Engineering, Faculty of Engineering, Universitas Indonesia, Indonesia.*
[2]*Department of Research and Innovation Infrastructure-BRIN, Cibinong, Indonesia.*

[*]**Corresponding author:** nelson@che.ui.ac.id

Original Research

Received:
2 January 2025
Revised:
11 March 2025
Accepted:
6 April 2025
Published online:
10 April 2025

Abstract:

Anodic plasma electrolysis, an advanced oxidation process (AOP), is an alternative method for synthesizing formic acid through the oxidation of methanol, known for producing a high amount of hydroxyl radicals ($OH^{\bullet}$). This study aims to synthesize formic acid using anodic plasma electrolysis at a high power setting of 500 W. In addition, it seeks to determine the effects of applied voltage and air injection flow rates on the formation of formic acid from methanol and ethanol feedstocks. The experimental setup involved injecting air through a cathode pipe into the anodic plasma zone in a Na_2SO_4 electrolyte solution. The process was conducted in a 1.2-L batch reactor, varying the voltage and air injection flow rates, using methanol and ethanol as feed materials. The highest yield of formic acid was 5.077 mmol from methanol oxidation and 7.268 mmol from ethanol oxidation after 45 minutes of reaction time. Optimal results were achieved at an applied voltage of 680 V, an air injection flow rate of 0.8 Lpm (L/min), a fixed power of 500 W, and a feed concentration of 2% v/v. The primary by-product identified was nitrate (NO_3^-), with 2.093 mmol generated from methanol oxidation and 2.281 mmol from ethanol oxidation. In addition, the morphology of the eroded stainless steel electrode revealed a mushroom-like shape with a rough and porous surface.

Keywords: Anodic plasma electrolysis; Formic acid; Methanol; Air injection; Radical OH

1. Introduction

Formic acid, a non-toxic, high-energy-density, and biodegradable carboxylic acid, is renowned for its wide utilization across various industries. It is used as a preservative in animal feed, a tanning agent in leather production, a dyeing additive in textiles, and a coagulant in rubber latex [1]. Global demand for formic acid witnessed a substantial increase of 750,000 tonnes in 2022 and is projected to continue growing at a rate of 4.48% [2].

Traditionally, formic acid production methods include hydrolysis of methyl formate, hydrocarbon oxidation, hydrolysis of formamide, and preparation from formate [3]. Among these, hydrolysis of methyl formate is the most commonly employed. However, these conventional methods suffer from drawbacks such as low efficiency, production of unwanted by-products, slow reaction rates, high energy consumption, and significant reliance on fossil fuels [3, 4]. Moreover, these processes emit approximately 2.18 tons of CO_2 per ton of formic acid produced, stemming from the formation of steam and syngas in the upstream stages of the formic acid formation process [5].

In recent years, researchers have explored alternative methods for producing formic acid, such as CO_2 photocatalytic synthesis, methanol oxidation, and electrocatalytic synthesis. For instance, Zhang et al. [6] reported the formation of formic acid via CO_2 photocatalysis using a graphene-TiO_2 catalyst, yielding 167.79 μmol/g of formic acid. Similarly, Fang et al. [7] achieved formic acid yields of $81-82\%$ through methanol oxidation using Fe-MOR heterogeneous catalysts. Wei et al. [8] further advanced this synthesis via the electrocatalytic method, employing CuONS/CF and mSnO_2/CC catalysts at the anode and cathode, respectively. The study resulted in Faraday efficiencies of 91.3% at the anode and 80.5% at the cathode. Despite their potential, these methods are hampered by challenges such as high operating conditions, excessive chemical usage, and complex catalyst preparation.

Plasma electrolysis presents a promising alternative, operating under ambient conditions and eliminating the need for excess chemicals. This method generates plasma by applying high voltage to electrodes immersed in a conductive electrolyte solution [9–11]. Plasma can form at the anode (anodic plasma) or the cathode (cathodic plasma), with anodic plasma being particularly effective for oxidation processes due to its higher production of •OH radicals. Anodic plasma electrolysis has been successfully applied in wastewater treatment [12] and carboxylic acid synthe-

sis [13]. Ito et al. [13] demonstrated the ability of anodic plasma electrolysis to oxidize methanol into formic acid under ambient conditions, achieving a 6.2% yield of formic acid using low power.

To our knowledge, no studies have explored the use of high-power plasma electrolysis for formic acid production. This research aims to address this gap by employing higher energy levels to improve formic acid yield through anodic plasma electrolysis. This study also aims to assess the impact of varying air injection flow rates, voltage, and feedstock (methanol and ethanol) on formic acid formation. The erosion and surface morphology of the plasma electrodes will also be analyzed, along with an investigation of by-products like nitrate.

2. Materials and methods

In this study, an anodic plasma electrolysis reactor was designed to synthesize formic acid from methanol, as shown in figure 1. The reactor consists of a glass vessel equipped with a DC diaphragm pump and an air-cooled condenser to maintain the system at an operating temperature of $50-55$ °C. The plasma electrode (anode) was made of stainless steel (AS SUS 316) shaped into a cylinder with a diameter of 1.6 mm and a length of 15 cm. The cathode, also made of stainless steel (AS SUS 316), was a pipe with a U-shaped end featuring a nominal diameter of $1/4$ inch and a length of 20 cm. The plasma electrodes were immersed to a depth of 5 mm, with a 1.0 cm gap between the anode and cathode ends.

The electrical setup for the reactor consisted of a multimeter, diode bridge, transformer setup, and slide regulator, all connected to an AC power source. The total solution volume in the system was 1.2 L, comprising 0.02 M Na_2SO_4 electrolyte and 2% v/v methanol.

The methanol oxidation process using an anodic plasma reactor was carried out at a fixed power of 500 W with several sets of operating conditions: (1) 640 V, 680 V, and 720 V applied voltages; (2) 0, 0.2, 0.4, and 0.8 Lpm air injection flow rates; and (3) methanol and ethanol as feedstocks. Samples were collected at intervals of 5, 10, 20, 30, and 45 minutes during the operation.

Each sample was analyzed using high-performance liquid chromatography (HPLC) to determine the concentration of formic acid produced. By-products, specifically nitrate compounds, were measured using the NitraVer reagent and analyzed with an ultraviolet-visible (UV-Vis) spectrophotometer. The erosion of the electrode material was assessed by measuring the mass of the electrode before and after the process. In addition, the morphological characterization of the eroded electrode was further examined using scanning electron microscopy-energy dispersive spectroscopy (SEM-EDS) analysis.

3. Results and discussion

In studying the anodic plasma electrolysis process, understanding the correlation between voltage and current is paramount for optimizing the efficiency and performance of formic acid synthesis. The variable voltage utilized in this process has been verified to occur in the glow discharge region of voltage–current characteristics. This section will further explore the effects of voltage, air injection, and feed types (methanol and ethanol) on formic acid formation. Additionally, the erosion of the plasma electrode, as well as the by-products, especially nitrate, will be examined.

3.1 Voltage-current characteristic

Figure 2 depicts a typical voltage–current curve for the plasma electrolysis process, focusing specifically on anodic plasma. This process is characterized by three distinct stages that lead to plasma electrolysis. The process begins with Faradaic electrolysis, which occurs in the ohmic zone and is known as normal electrolysis. During this stage, small gas bubbles are liberated at both electrodes and the current increases linearly with the increasing voltage [14]. As the voltage increases further, the resultant Joule heating induces local vaporization of the electrolyte solvent adjacent to the smaller electrode. This leads to the coalescence of fine vapor bubbles, which form a sustained, pulsating, thin vapor gas envelope surrounding the anode. Faradaic electrolysis will be terminated upon the beginning of gas–vapor sheath formation, marking the onset of the transitional phase [14, 15].

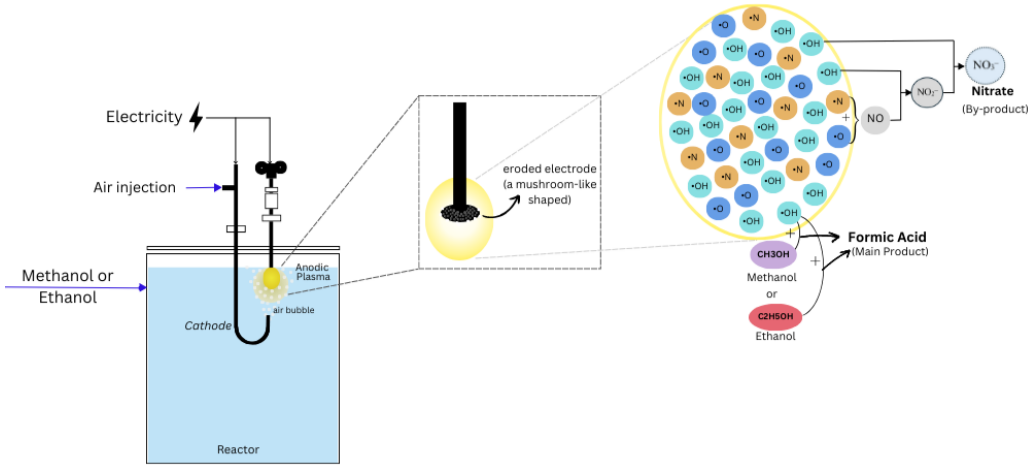

Figure 1. Experimental setup of anodic plasma electrolysis reactor by air injection for formic acid production.

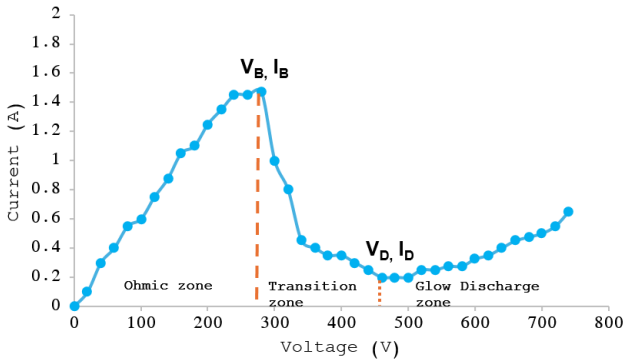

Figure 2. The voltage–current characteristic without air injection on anodic plasma electrolysis using stainless steel as plasma electrode and 0.02 M Na_2SO_4 as electrolyte.

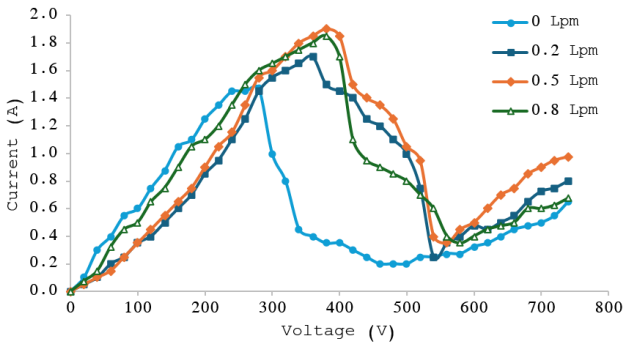

Figure 3. The voltage–current characteristic with varying air injection rates using stainless steel as plasma electrode and 0.02 M Na_2SO_4 as electrolyte.

The curve's maximum point, known as the breakdown point, is where the maximum current (I_B) of 1.45 A begins to decrease as the voltage (V_B) increases to 280 V. The maximum energy at this point, referred to as breakdown energy (E_B), is 413 J/s.

When the applied voltage exceeds the breakdown point threshold, the process enters the transitional phase. During this phase, the gas–vapor envelope surrounding the discharge electrode thickens, resulting in a decrease in electric current due to the increased electrical resistance within the gas and vapor in the envelope [14, 15]. The increased voltage during this phase becomes sufficiently high to initiate ionization of the gas–vapor envelope. As this phase ends, the ionization of the gas vapor in the envelope transitions into an electrical discharge and ignites a small and unstable spark at the electrode tip. This phase concludes at the curve's minimum point, known as the discharge onset point. As the voltage increases further beyond the discharge voltage (V_D) of over 460 V, the current rises from the minimum current, or discharge current (I_D), of 0.2 A. The glow discharge, which started as a small spark, now extends across the entire submerged electrode, becoming stable and brighter [14, 15].

3.2 Effect of Air injection on voltage-current characteristic

According to figure 3 and Table 1, the V_B in the absence of air injection (280 V) is lower than that with the air injection (360 – 380 V) variable. This difference arises due to the decreased electrolyte temperature caused by the air injection bubbles. Plasma formation typically favors high temperatures around the plasma electrode or electrolyte. However, the introduction of air injection reduces the temperature around the anode, making the Joule heating evaporation effect more challenging to achieve. Consequently, forming a gas envelope requires more energy. This phenomenon aligns with Sengupta et al. [16], who noted that lower electrolyte temperatures demand a higher Joule heating effect for local evaporation, leading to a more prolonged and challenging gas sheath formation at the electrodes, where the normal electrolysis process will stop upon reaching its maximum current (I_B, V_B). Therefore, the V_B value is lower in the absence of air injection because the electrolyte temperature remains higher and more homogeneous around the plasma electrode, allowing for quicker local evaporation by Joule heating and easier sheath formation.

In the transition zone, the absence of air injection results in a very significant decrease in current compared to that in the presence of air injection. This decrease in current is due to the formation of a thicker and more continuous gas sheath, which increases the electrical resistance between the gas sheath and the electrolyte. By contrast, air injection disrupts the stability of the gas sheath, causing random and unstable interactions between the evaporation process bubbles and the air injection bubbles, leading to a gradual decrease in current in the air injection variable. Therefore, air injection requires more energy to establish a stable gas sheath.

Meanwhile, at the discharge onset point (I_D, V_D), the presence of air injection complicates the formation of a complete plasma flame. The air injection bubbles contribute to plasma flame instability, often resulting in its disappearance. This instability necessitates a higher glow discharge current (I_D) and glow discharge energy (E_D) to stabilize the plasma. Regarding the air injection flow rate, a 0.5 Lpm air injec-

Table 1. Comparison of V_B, I_B, V_D, and I_D on air injection flowrate variation.

Air injection flow rate	Breakdown condition			Discharge condition		
(Lpm)	V_B (V)	I_B (A)	E_B (J/s)	V_D (V)	I_D (A)	E_D (J/s)
0	280	1.475	413	460	0.2	92
0.2	360	1.7	612	540	0.25	135
0.5	380	1.9	722	560	0.35	196
0.8	380	1.85	703	580	0.35	203

tion flow rate produces higher V_B and E_B values (380 V and 722 J/s) than a 0.2 Lpm flow rate (360 V and 612 J/s). Increasing the air injection flow rate introduces two factors: a more significant decrease in electrolyte temperature around the plasma electrode and increased disturbance in the stability of the gas sheath. The first factor involves a greater reduction in electrolyte temperature with a higher air injection flow rate, making the Joule heating evaporation process more difficult and the formation of a gas sheath more energy-intensive.

The second factor relates to the disruption of gas sheath stability by air injection bubbles. A higher air injection flow rate increases the shear velocity between the liquid and air layers, causing a greater disturbance at the liquid-air interface, as characterized by waves in the liquid-gas layer. This disturbance makes it more challenging to form a gas sheath, consistent with the Kelvin-Helmholtz instability theory, which states that shear velocity at the interface of two fluid layers can cause instability and wave formation in the interface layer [17]. Therefore, a higher air injection flow rate makes gas sheath formation more difficult, requiring more energy.

At the onset of discharge, the discharge energy (E_D) at a flow rate of 0.8 Lpm (203 J/s) exceeds that of the airflow rates of 0.2 and 0.5 Lpm, corresponding to 135 J/s and 196 J/s, respectively. This discrepancy may be attributed to higher airflow rates destabilizing the formed plasma, necessitating greater energy input to achieve a stable and luminous plasma flame. Therefore, selecting an appropriate airflow rate is crucial for optimal performance.

3.3 Effect of voltage on formic acid synthesis

Voltage testing was conducted within the 640 – 720 V range, as determined through the analysis of the voltage–current characterization depicted in figure 2. This range falls within the glow discharge zone. The study results shown in figure 4 demonstrate the amount of formic acid produced in this voltage variation.

Figure 4 shows a clear positive correlation between the quantity of formic acid generated and the applied voltage. Specifically, the amounts of formic acid produced were 3.742, 5.077, and 5.088 mmol at 640, 680, and 720 V, respectively. This correlation highlights the influence of applied voltage on plasma intensity, as increased voltage results in increased plasma intensity, observable through the size of the plasma flame, as demonstrated by the varying sizes of the plasma flame shown in Figure 5. The comparative analysis indicates that the plasma flame at 640 V is considerably smaller than those at 680 V and 720 V, leading to a reduced formic acid yield at the lower voltage (Figure 4).

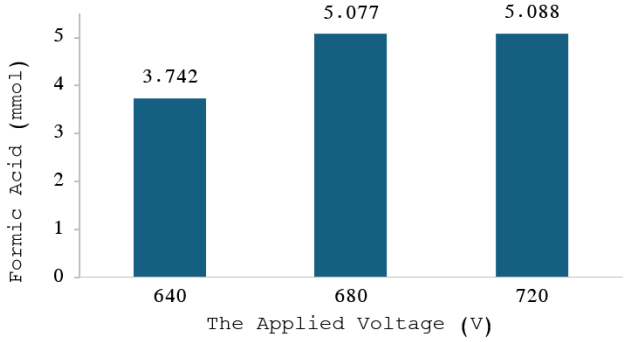

Figure 4. Formic acid formation at varying applied voltages by anodic plasma electrolysis (0.8 Lpm air injection flow rate; 2% v/v methanol; 45-minute operating time).

The plasma flame size in the plasma electrolysis process indicates the number of high-energy electrons excited by increasingly intense and rapid electron collisions. As supported by Yan et al. [18], increased voltage results in higher electron density, which enhances collision intensity, leading to faster and more stable plasma with a brighter flame [18]. This brighter plasma, in turn, produces a greater number and variety of active radical species, such as $^{\bullet}$O and $^{\bullet}$OH [19]. The $^{\bullet}$OH radicals formed in this process are particularly vital in the production of formic acid, thus explaining the increased yields at higher voltages.

Based on figure 4, the highest formic acid yield of 5.088 mmol was obtained at 720 V. However, the marginal increase from 680 V to 720 V (only 0.011 mmol) suggests that the voltage might have reached an optimal point. Beyond this point, further voltage increases result in more constant production of $^{\bullet}$OH radicals, thereby stabilizing the formic acid yield. This phenomenon is corroborated by the current–voltage characterization curve in figure 2, which shows similar current values for 680 V (0.6 A) and 720 V (0.625 A) at an air injection flow rate of 0.8 Lpm. The comparable plasma flames at these voltages depicted in figure 5 reinforce this observation. Consequently, 680 V will be selected for the next stage, as the associated process risk is lower compared to 720 V.

3.4 Effect of air injection flow rate on formic acid synthesis

In this study, the direct injection of air from the cathode to the anode plasma influences the formation of formic acid. The research results depicted in figure 6 below show the amount of formic acid produced at each air injection flow rate.

The addition of air affects the amount of formic acid formed. Air, which is predominantly composed of oxygen, facilitates the generation of various reactive oxygen species (ROS) in substantial quantities during the plasma electrolysis process. These ROS include singlet oxygen atoms ($^1O_2$), atomic oxygen radicals ($^{\bullet}$O), hydroxyl radicals ($^{\bullet}$OH), and superoxide radicals ($O_2^{\bullet-}$). These ROS indirectly enhance the production of formic acid by serving as precursors that can be converted into $^{\bullet}$OH radicals. The $^{\bullet}$OH radical, known for its potent oxidizing capabilities, is highly effective in oxidizing aliphatic alcohol compounds like methanol. The generation of $^{\bullet}$OH radicals from ROS can be represented by equations 1–8 [20].

(1) $O_2 + e^* \rightarrow {}^{\bullet}O + {}^{\bullet}O + e^-$

(2) ${}^{\bullet}O + H_2O_{(l)} \rightarrow {}^{\bullet}OH + {}^{\bullet}OH$

(3) $O_2 + e^- \rightarrow O(^3P) + O(^1D)$

(4) $O(^1D) + H_2O \rightarrow 2\ {}^{\bullet}OH$

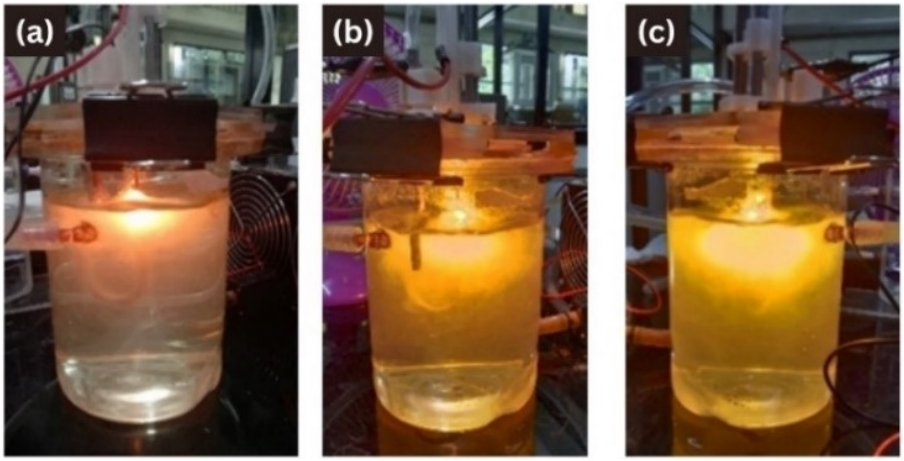

Figure 5. Plasma flames on anodic plasma electrolysis at (a) 640 V, (b) 680 V, and (c) 720 V.

(5) $O_2 + {}^{\bullet}H \rightarrow {}^{\bullet}OH + {}^{\bullet}O$

(6) $O_2 + e^- \rightarrow O_2^{\bullet -}$

(7) $2O_2^{\bullet -} + 2H^+ \rightarrow O_2 + H_2O_2$

(8) $H_2O_2 + e^- \rightarrow {}^{\bullet}OH + OH^-$

Looking at figure 6, the formic acid formed with air injection is greater (4.577 mmol) than that without (3.685 mmol). This could be due to ROS species acting as precursors of $^{\bullet}$OH radicals when air is added. The presence of these ROS species facilitates the formation of more $^{\bullet}$OH radicals, not just from the dissociation of water and methanol molecules but also through additional pathways, thereby augmenting formic acid production. Meanwhile, the speciation of $^{\bullet}$OH radicals produced in the variable without air injection only comes from the dissociation of water and methanol molecules.

Based on figure 6, the production of formic acid consistently rises with an increase in the air injection flow rate. A higher airflow rate leads to the dissociation of a larger quantity of oxygen compounds in the system, resulting in an elevated formation of ROS species. These ROS species, in turn, produce more $^{\bullet}$OH radicals during the plasma electrolysis process (as represented by equations 1–8), thereby boosting the formation of formic acid.

When comparing airflow rates of 0.2 and 0.5 Lpm, the production of formic acid remains relatively constant, with a minimal difference of 0.06 mmol. This observation suggests a potential instability in plasma formation at 0.5 Lpm flow rate, resulting in a smaller plasma and a nearly equivalent generation of ROS reactive species compared to 0.2 Lpm flow rate. However, the increase in formic acid production to 5.077 mmol at 0.8 Lpm airflow rate is noteworthy. This substantial rise can be attributed to the continuous air injection at this flow rate, which results in a thicker gas envelope, greater plasma stability, and an increased generation of radical species, particularly $^{\bullet}$OH radicals, thereby enhancing methanol oxidation. Therefore, the most effective air injection flow rate for maximizing formic acid production is identified as 0.8 Lpm, yielding 5.077 mmol of formic acid.

3.5 Effect of methanol and ethanol feed on formic acid synthesis

This study was further extended to investigate the effects of methanol and ethanol feed on the amount of formic acid formation, as shown in figure 7.

Methanol, one of the shortest C molecular chains of alcohol, exhibits higher reactivity compared to other aliphatic alcohols, leading to an accelerated ionization process and a more rapid oxidation process by $^{\bullet}$OH radicals. The synthesis of formic acid through this process follows second-order reac-

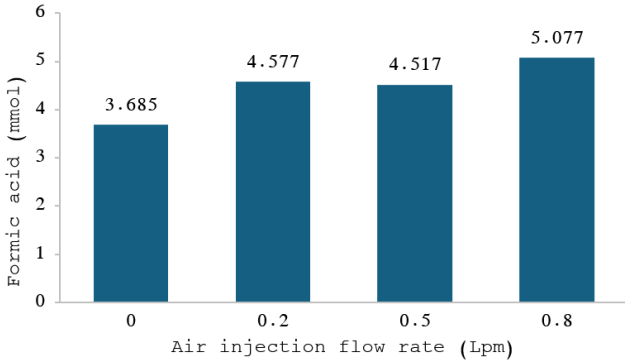

Figure 6. Formic acid formation at varying air injection flow rates by anodic plasma electrolysis (680 V, 2% v/v methanol, and 45-minute operating time).

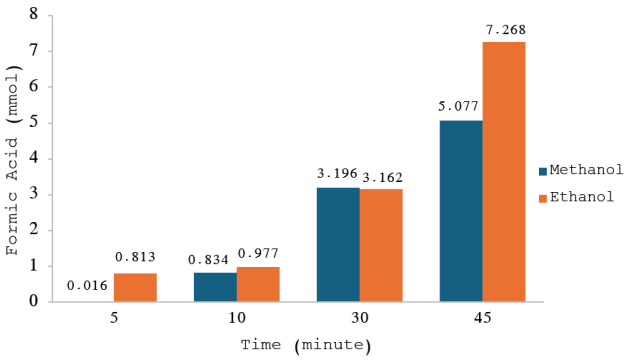

Figure 7. Formic acid formation with varied feeds (methanol and ethanol) by anodic plasma electrolysis (680 V; 0.8 Lpm air injection flow rate; 2% v/v feed concentration).

tion kinetics, meaning that the availability of both methanol feed and $^{\bullet}OH$ radicals significantly influences the formation of formic acid. This dynamic is reflected in the substantial increase in formic acid yield from methanol, reaching 5.077 mmol at 45 minutes (figure 7).

A similar pattern is observed with ethanol, which is the next most reactive aliphatic alcohol after methanol. The reactivity of ethanol to $^{\bullet}OH$ hastens the oxidation process during plasma electrolysis. However, in the initial 5 to 10 minutes, the formic acid yield remains relatively constant, with only a difference of 0.164 mmol. This could be due to the complex and branched reaction pathway required for ethanol to convert into formic acid, necessitating more time for its formation. This phenomenon is consistent with the results of this study, where, at longer operating times of 30 to 45 minutes, formic acid production significantly increased, reaching 3.162 and 7.268 mmol, respectively (figure 7). The mechanism for formic acid formation from ethanol is outlined in equations 9–12 [21, 22].

When comparing both feeds (methanol and ethanol), as shown in figure 7, ethanol results in a higher formic acid yield of 7.268 mmol compared to methanol's 5.077 mmol. The oxidation of ethanol by $^{\bullet}OH$ tends to produce a larger quantity of radical species that contribute to the formation of formic acid. This is attributed to ethanol's longer C-H chains, which generate a greater variety of radical species through the breaking of hydrogen atoms in C-H bonds. The associated reactions can be described using equations 9–12.

$$(9)\quad CH_3CH_2OH + {}^{\bullet}OH \rightarrow CH_3{}^{\bullet}CHOH + H_2O$$

$$(10)\quad CH_3{}^{\bullet}CHOH + O_2 \rightarrow CH_3C(OO^{\bullet})HOH$$

The radical α-hydroxyethylperoxy obtained from equation 10 can undergo direct dissociation into acetaldehyde compounds and hydroperoxyl radicals ($^{\bullet}HO_2$), as shown in equation 11a. However, in the presence of NO_x ($NO + NO_2$) compounds, which are produced by nitrogen compounds from the air, the α-hydroxyethylperoxy radical reacts faster with NO compounds and forms the α-hydroxyethyloxyl radical ($CH_3CH(O^{\bullet})OH$) and NO_2, as shown in equation 11b.

This phenomenon was investigated by da Silva and Bozzelli [22], who found that at NO concentrations as low as ~ 10 ppb, the α-hydroxyethylperoxy radical preferentially reacts with NO, outpacing its own decomposition (equation 11).

$$(11a)\quad CH_3C(OO^{\bullet})HOH \rightarrow CH_3CHO + HO_2^{\bullet}$$

$$(11b)\quad CH_3C(OO^{\bullet})HOH + NO \rightarrow CH_3CH(O^{\bullet})OH + NO_2$$

$$(12a)\quad CH_3CH(O^{\bullet})OH \rightarrow HCOOH + {}^{\bullet}CH_3$$

$$(12b)\quad CH_3CH(O^{\bullet})OH \rightarrow CH_3COOH + {}^{\bullet}H$$

The α-hydroxyethyloxyl radicals produced in this process can dissociate into either formic acid + $^{\bullet}CH_3$ or acetic acid + $^{\bullet}H$, as demonstrated in equation 12. However, due to the exothermic conditions present in this study, the decomposition of oxyl radicals is more likely to favor the formation of formic acid and $^{\bullet}CH_3$ radicals. This preference is driven by the higher enthalpy of formation of formic acid and $^{\bullet}CH_3$ radicals, which is 4.8 kcal/mol, compared to the 0.3 kcal/mol for acetic acid and $^{\bullet}H$ radicals [22]. Therefore, the presence of NO compounds in the system introduces a new reaction pathway that enhances the formation of formic acid.

3.6 Erosion of stainless steel as plasma electrode

In this study, the morphology of the eroded surface of the plasma electrode tip was also observed using scanning electron microscopy (SEM). Initially, before the plasma electrolysis process began, the surface of the stainless steel electrode tip appeared relatively smooth, with a uniform structure and visible streak lines (figure 8 (1)). However, after the plasma electrolysis process, a significant transformation was observed on the electrode surface, as shown in figure 8 (2).

The stainless steel electrode exhibits a swelling at the tip, resembling a mushroom morphology (figure 8 (2a)). This swelling is likely attributed to the formation of a protective oxide layer that mitigates erosion of the stainless steel electrode during the plasma electrolysis process [23]. When the

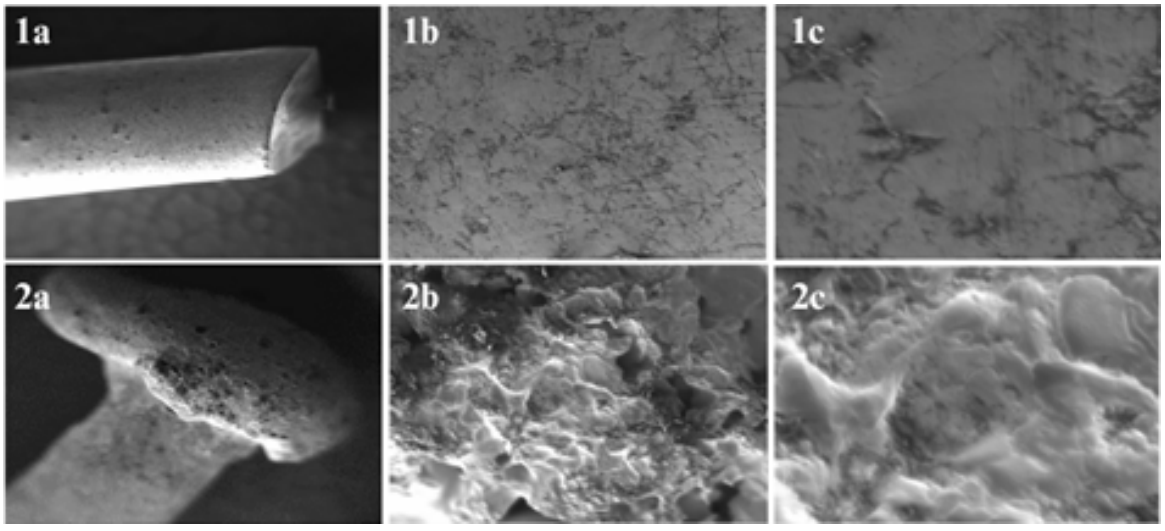

Figure 8. The surface morphology of stainless steel electrode: (1) before anodic plasma electrolysis and (2) after plasma electrolysis with magnification at (a) 55x, (b) 500x, and (c) 1500x.

stainless steel electrode comes into contact with oxygen, the metal elements within it react to form a metal oxide layer on the electrode surface. This oxide layer acts as a barrier, protecting the underlying metal from further degradation.
The energy dispersive spectroscopy (EDS) mapping results in figure 8 reveal that the composition of Fe, Cr, and O is more concentrated, as indicated by the higher brightness and density of points in the EDS map, compared to Mo, Ni, and C. This suggests that the surface of the stainless steel electrode is predominantly covered by Fe and Cr oxide layers, providing additional evidence of the protective nature of the oxide layer formed during the plasma electrolysis process.
The EDS composition spectra depicted in figure 9 reveal detailed insights into the elemental composition of the stainless steel electrode before and after plasma electrolysis. The outermost layer (figure 10 (3) and Table 2) exhibits a composition of 52.16% wt Fe, 30.44% wt O, and 3.47% wt Cr. Similarly, the grey area (figure 10 (2) and Table 2) displays a composition of 52.97% wt Fe, 35.15% wt O, and 2.83% wt Cr. The substantial presence of Fe in these layers indicates its strong propensity to migrate toward the electrode surface relative to Cr.
The Fe oxide layer, observed to be more porous and brittle due to the high heat intensity of the plasma [23], is evident in figures 8 (2b–2c) at 500x and 1500x magnifications. Conversely, Cr forms a dense and robust CrO_2 layer, serving as a passivation layer that effectively reduces further erosion of the electrode surface [23].
The EDS analysis provides insights into the composition of the stainless steel electrode, as presented in figure 10 and Table 2. The 30.44% wt of element O is attributed to the metal oxide layer resulting from the reaction with oxygen during the plasma electrolysis process. The composition of Cr, Ni, and Mo originates from the stainless steel electrode, which initially contained 68.5% Fe, 0.08% C, 2% Mn, $16-18$% Cr, $10-14$% Ni, and $2-3$% Mo [24].
Meanwhile, the innermost layer, characterized by black areas, shows the highest amount of carbon (C) composition, suggesting a carbonation effect on the electrode during plasma electrolysis. This effect is likely due to carbon compounds in the methanol reactants, which contribute to the observed carbon deposition.

3.7 Analysis of nitrate formation as by-product of anodic plasma electrolysis

Apart from the main product, which is formic acid, nitrate compounds are also produced as by-products in the plasma electrolysis process. This study investigates nitrate formation, given that air injection—comprising approximately 78% nitrogen—introduces nitrogen compounds into the system. This study used stainless steel plasma electrodes and operated under the following conditions: fixed power of 500 W, voltage of 680 V, air injection flow rate of 0.8 Lpm, and methanol concentration of 2% v/v. Measurements of nitrate compounds were limited to the liquid phase and conducted at operating times of 5, 10, 20, 30, and 45 minutes.
Air injection, containing 78% nitrogen and 21% oxygen, is effective in forming various radical species in the liquid phase, including $^{\bullet}O$, $^{\bullet}OH$, $^{\bullet}N$, $^{\bullet}N_2^*$, $^{\bullet}N_2^+$, and $^{\bullet}H$ [25]. These radical species form through molecular activation by high-energy electrons or interactions with other radicals during the plasma process. These reactive species can subsequently lead to the formation of nitrate compounds [25].
Comparative data on the concentration of nitrate compounds from the oxidation of methanol and ethanol are presented in Table 3.
According to Table 3, the concentration of detected nitrate compounds increases with extended process duration. This increase is attributed to the air injection rate being kept constant for 45 minutes, which ensures a continuous supply of nitrogen and oxygen compounds. Regarding feed variations, the nitrate yield from ethanol (2.281 mmol) was higher than methanol (2.093 mmol) after 45 minutes. This phenomenon occurs because most of the NO compounds formed during plasma electrolysis are more readily converted into NO_2 compounds when they bind to the α-hydroxyethyl peroxy radical (equation 11b) in ethanol oxidation [22]. As a result, the higher production of NO_2 compounds in ethanol oxidation leads to increased nitrate formation.
The quantity of nitrate compounds obtained as a by-product in this process (2.093 mmol) is immensely lower than the formic acid yield (5.077 mmol) from methanol oxidation. This discrepancy is due to the more favorable free Gibbs

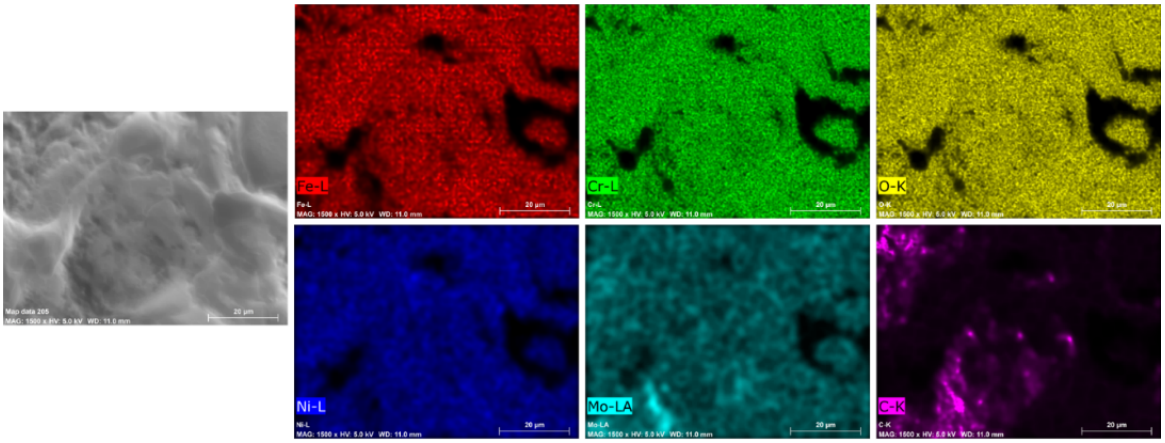

Figure 9. EDS mapping of the stainless steel electrode's surface.

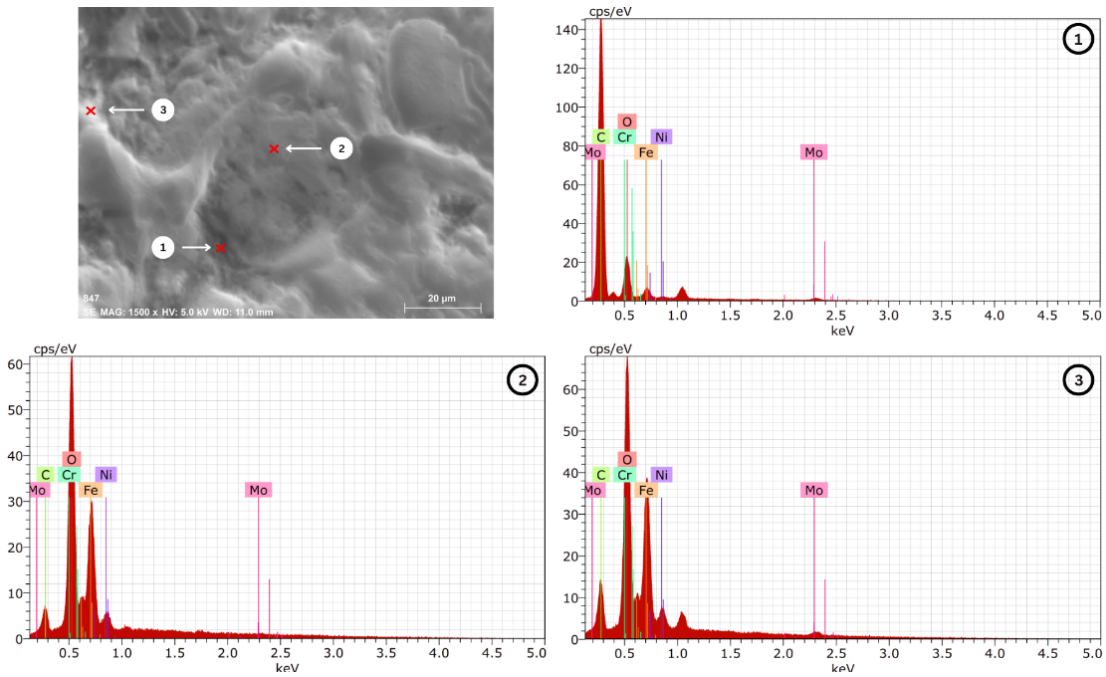

Figure 10. EDS spectra of the stainless steel electrode's surface: (1) innermost part–black area, (2) middle part–grey area, and (3) outermost part–white area.

energy for methanol oxidation compared to nitrate synthesis. The free Gibbs energy of methanol oxidation to formic acid is −471.8 kJ/mol, indicating a more spontaneous process, while nitrate synthesis has a Gibbs energy of −111.3 kJ/mol [26].

4. Conclusion

This study demonstrates the successful synthesis of formic acid through anodic plasma electrolysis from the oxidation of methanol and ethanol. The optimal operating conditions identified are an applied voltage of 680 V, an air injection flow rate of 0.8 Lpm, and a 2% v/v methanol concentration, resulting in 5.077 mmol of formic acid after 45 minutes. Ethanol oxidation yields a higher amount of formic acid (7.268 mmol) compared to methanol oxidation (5.077 mmol) due to the greater diversity of radical species formed during ethanol oxidation, which enhances formic acid production.

The morphology of the eroded stainless steel electrode tip reveals mushroom-like swelling. This is attributed to the formation of a protective layer of CrO_2 that prevents further erosion during the anodic plasma electrolysis process. The by-products obtained were nitrate (NO_3^-) compounds, with quantities of 2.093 mmol and 2.281 mmol from methanol and ethanol oxidation, respectively. The formation of these nitrate compounds as by-products is linked to the presence of nitrogen-rich air injection.

Table 2. Composition of various elements on the eroded stainless steel surface after anodic plasma electrolysis based on EDS spectra

Stainless steel electrode surface	Composition of elements (%wt)					
Outermost part	52.16	3.47	30.44	5.83	6.12	1.98
Middle part	52.97	2.83	35.15	3.06	5.46	0.53
Innermost part	10.01	1.68	16.14	67.79	1.18	3.20

Table 3. Nitrate formation as a by-product of formic acid production in methanol and ethanol feedstocks.

Operating time (minutes)	Nitrate produced (mmol)	
	Methanol feed	Ethanol feed
5	0.133	1.433
10	0.227	1.603
20	0.508	1.961
30	1.830	2.207
45	2.093	2.281

Acknowledgment
This study was funded by Publikasi Terindeks International Pasca Sarjana under Contract No. NKB-124/UN2.RST/HKP.05.00/2024 from the Directorate of Research and Community Service, Universitas Indonesia.

Authors Contribution
Triana Devi Sijabat: Writing–original draft, Writing–review & editing, Conceptualization, Visualization, Investigation, Data Curation, Software. Nelson Saksono: Writing–review & editing, Conceptualization, Methodology, Supervision, Validation, Visualization, Project administration, Funding acquisition. Bening Farawan: Formal analysis, Investigation, Resources, Supervision, Software.

Availability of data and materials
The data that support the findings of this study are available from the corresponding author, upon reasonable request.

Conflict of interests
The authors declare that they have no known competing financial interests or personal relationships that could have appeared to influence the work reported in this paper.

References

[1] X. Liu, S. Li, Y. Liu, and Y. Cao. "Formic acid: A versatile renewable reagent for green and sustainable chemical synthesis. ". *Chinese Journal of Catalysis*, **36**:1461–1475, 2015.
DOI: https://doi.org/10.1016/S1872-2067(15)60861-0.

[2] B. Thijs, J. Rongé, and J. A. Martens. "Matching emerging formic acid synthesis processes with application requirements. ". *Green Chemistry*, **24**:2287–2295, 2022.
DOI: https://doi.org/10.1039/D1GC04791D.

[3] J. Hietala, A. Vuori, P. Johnsson, I. Pollari, W. Reutemann, and H. Kieczka. "Formic acid. In: Ullmann's Encyclopedia of Industrial Chemistry.". *Wiley*, pages 1–22, 2016.
DOI: https://doi.org/10.1002/14356007.a12_013.pub3.

[4] M. Rumayor, A. Dominguez-Ramos, and A. Irabien. "Formic acid manufacture: Carbon dioxide utilization alternatives.". *Applied Radiation and Isotopes*, **8**, 2018.
DOI: https://doi.org/10.3390/app8060914.

[5] M. Pérez-Fortes and E. Tzimas. "Techno-economic and environmental evaluation of CO_2 utilisation for fuel production: Synthesis of methanol and formic acid. ". *Synthesis of Methanol and Formic Acid*, 2016.
DOI: https://doi.org/10.2790/981669.

[6] Q. Zhang, C. F. Lin, Y. H. Jing, and C. T. Chang. "Photocatalytic reduction of carbon dioxide to methanol and formic acid by graphene-TiO_2.". *Journal of the Air and Waste Management Association*, **64**: 578–585, 2014.
DOI: https://doi.org/10.1080/10962247.2013.875958.

[7] Z. Fang, H. Murayama, Q. Zhao, B. Liu, F. Jiang, Y. Xu, M. Tokunaga, and X. Liu. "Selective mild oxidation of methane to methanol or formic acid on Fe-MOR catalysts.". *Catalysis Science and Technology*, **9**:6946–6956, 2019.
DOI: https://doi.org/10.1039/c9cy01640f.

[8] X. Wei, Y. Li, L. Chen, and J. Shi. "Formic acid electro-synthesis by concurrent cathodic CO_2 reduction and anodic CH_3OH oxidation.". *Angewandte Chemie International Edition*, **60**:3148–3155, 2021.
DOI: https://doi.org/10.1002/anie.202012066.

[9] P. Gupta, G. Tenhundfeld, E. Daigle, and D. Ryabkov. "Electrolytic plasma technology: Science and engineering-An overview. ". *Surface and Coatings Technology*, **201**:8746–8760, 2007.
DOI: https://doi.org/10.1016/j.surfcoat.2006.11.023.

[10] M. A. Almubarak and A. Wood. "Chemical action of glow discharge electrolysis on ethanol in aqueous solution.". *ECS*, **124**, 1977.

[11] A. Hickling and M. D. Ingram. "Glow-discharge electrolysis. ". *Journal of Electroanalytical Chemistry*, **8**:65–81, 1964.
DOI: https://doi.org/10.1016/0022-0728(64)80039-5.

[12] N. Saksono, P. Suryawinata, Z. Zakaria, and B. Farawan. "Fixation of air nitrogen to ammonia and nitrate using cathodic plasma and anodic plasma in the air plasma electrolysis method.". *Environmental Progress & Sustainable Energy*, **43**, 2023.
DOI: https://doi.org/10.1002/ep.14331.

[13] Y. Ito, T. Munegumi, and K. Harada. "Synthesis of carboxylic acids from alcohols by contact glow discharge with recycling system. ". *Research Journal of Pharmaceutical, Biological and Chemical Science*, **4**:1811–1818, 2013.

[14] S. K. S. Gupta and R. Singh. "Cathodic contact glow discharge electrolysis: Its origin and non-faradaic chemical effects.". *Plasma Sources Science and Technology*, **26**:015005–1–015005–8, 2016.

[15] S. Bespalko and J. Mizeraczyk. "Overview of the hydrogen production by plasma-driven solution electrolysis.". *Energies*, **22**:7508, 2022.
DOI: https://doi.org/10.3390/en15207508.

[16] S. K. Sengupta, A. K. Srivastava, and R. Singh. "Contact glow discharge electrolysis: a study on its origin in the light of the theory of hydrodynamic instabilities in local solvent vaporisation by Joule heating during electrolysis.". *Journal of Electroanalytical Chemistry*, **427**:23–27, 1997.
DOI: https://doi.org/10.1016/S0022-0728(96)05044-9.

[17] M. Sementilli, R. Zangeneh, and J. Chen. "Influence of cross perturbations on turbulent Kelvin–Helmholtz instability.". *Fluids*, **9**:52, 2024.
DOI: https://doi.org/10.3390/fluids9030052.

[18] Z. C. Yan, C. Li, and W. H. Lin. "Hydrogen generation by glow discharge plasma electrolysis of methanol solutions. ". *International Journal of Hydrogen Energy*, **34**:48–55, 2009.
DOI: https://doi.org/10.1016/j.ijhydene.2008.09.099.

[19] Y. Liu, B. Sun, L. Wang, and D. Wang. "Characteristics of light emission and radicals formed by contact glow discharge electrolysis of an aqueous solution.". *Plasma Chemistry and Plasma Processing*, **32**:359–368, 2012.
DOI: https://doi.org/10.1007/s11090-011-9347-7.

[20] M. Lu, W. Yang, C. Yu, Q. Liu, and D. Ye. "Plasma-catalytic oxidation of toluene on Ag-modified FeOx/SBA-15.". *Aerosol and Air Quality Research*, **20**:193–202, 2020.
DOI: https://doi.org/10.4209/aaqr.2019.09.0467.

[21] D. S. Levko, A. N. Tsymbalyuk, and A. I. Shchedrin. "Plasma kinetics of ethanol conversion in a glow discharge.". *Plasma Physics Reports*, **38**:913–921, 2012.
DOI: https://doi.org/10.1134/S1063780X1210008X.

[22] G. da Silva and J. W. Bozzelli. "Role of the α-hydroxyethylperoxy radical in the reactions of acetaldehyde and vinyl alcohol with HO_2.". *Chemical Physics Letters*, **483**:25–29, 2009.
DOI: https://doi.org/10.1016/j.cplett.2009.10.045.

[23] J. Heo, J. Lee, S. Kim, A. Alfantazi, and S. O. Cho. "Corrosion resistance of austenitic stainless steel using cathodic plasma electrolytic oxidation. ". *Surface and Coatings Technology*, **462**, 2023.
DOI: https://doi.org/10.1016/j.surfcoat.2023.129448.

[24] J. R. Davis. "Stainless steels.". *ASM International Handbook Committee*, 1994.

[25] N. Saksono, H. Harianingsih, B. Farawan, V. Luvita, and Z. Zakaria. "Reaction pathway of nitrate and ammonia formation in the plasma electrolysis process with nitrogen and oxygen gas injection. ". *Journal of Applied Electrochemistry*, **53**:1183–91, 2023. DOI: https://doi.org/10.1007/s10800-023-01849-4.

[26] R. Kleerebezem and S. Lücker. "Cyclic conversions in the nitrogen cycle.". *Frontiers in Microbiology*, **12**:622504, 2021. DOI: https://doi.org/10.3389/fmicb.2021.622504.